NANO · MICRO small
www.small-journal.com

Protein Corona Sensor Array Nanosystem for Detection of Coronary Artery Disease

*Gha Young Lee, Andrew A. Li, Intae Moon, Demos Katritsis, Yoannis Pantos, Francesco Stingo, Davide Fabbrico, Roberto Molinaro, Francesca Taraballi, Wei Tao, and Claudia Corbo**

Coronary artery disease (CAD) is the most common type of heart disease and represents the leading cause of death in both men and women worldwide. Early detection of CAD is crucial for decreasing mortality, prolonging survival, and improving patient quality of life. Herein, a non-invasive is described, nanoparticle-based diagnostic technology which takes advantages of proteomic changes in the nano-bio interface for CAD detection. Nanoparticles (NPs) exposed to biological fluids adsorb on their surface a layer of proteins, the "protein corona" (PC). Pathological changes that alter the plasma proteome can directly result in changes in the PC. By forming disease-specific PCs on six NPs with varying physicochemical properties, a PC-based sensor array is developed for detection of CAD using specific PC pattern recognition. While the PC of a single NP may not provide the required specificity, it is reasoned that multivariate PCs across NPs with different surface chemistries, can provide the desirable information to selectively discriminate the condition under investigation. The results suggest that such an approach can detect CAD with an accuracy of 92.84%, a sensitivity of 87.5%, and a specificity of 82.5%. These new findings demonstrate the potential of PC-based sensor array detection systems for clinical use.

1. Introduction

Cardiovascular disease (CVD) encompasses a group of diseases involving dysfunctions of the heart and/or blood vessels, representing the leading global cause of mortality.[1] In 2019, CVDs were a leading cause of death globally with the number of CVD death steadily increasing every year and amounting to nearly 18.6 million.[2] Coronary Artery Disease (CAD), which may lead to chronic and acute myocardial infarction, is the most common type of CVD. In 2017, ≈9 million deaths globally were attributed to CAD alone.[3] The projection for the next two decades estimated that the number of people with CAD will increase by more than 40% and that CAD will cause a total of ≈11 million deaths globally.[4] Management of CAD requires heavy economic costs, representing a major economic burden on public health. Overall, medical management of CAD in the

G. Y. Lee, W. Tao
Center for Nanomedicine
Department of Anesthesiology
Brigham and Women's Hospital
Harvard Medical School
Boston, MA 02115, USA

A. A. Li
Tepper School of Business
Carnegie Mellon University
Pittsburgh, PA 15213, USA

I. Moon
Department of Electrical Engineering and Computer Science
Massachusetts Institute of Technology
Cambridge, MA 4307, USA

D. Katritsis, Y. Pantos
Comprehensive Cardiology Care at Hygeia Hospital
Athens 15123, Greece

D. Katritsis
Johns Hopkins Medicine
Baltimore, MD 21287, USA

F. Stingo, D. Fabbrico
Department of Statistics
Computer Sciences and Applications
University of Florence
Florence 50121, Italy

R. Molinaro
Department of Cardiovascular
Brigham and Women's Hospital
Harvard Medical School
Boston, MA 02115, USA

F. Taraballi
Center for Musculoskeletal Regeneration
Houston Methodist Academic Institute & Orthopedics and Sports Medicine
Houston Methodist Hospital
Houston, TX 77030, USA

The ORCID identification number(s) for the author(s) of this article can be found under https://doi.org/10.1002/smll.202306168

DOI: 10.1002/smll.202306168

USA is estimated to cost $100 billion annually including therapeutics, medical management, and the cost from the loss of productivity from a sicker population.[5]

CAD, characterized by the presence of atherosclerotic plaques in the coronary arteries,[6] is a chronic condition that starts during adolescence and progresses gradually over one's lifetime. Atherosclerosis, the pathogenic process driving CAD, is instigated by endothelial dysfunction triggered by stress stimuli and inflammatory factors (e.g., oxidative stress and hemodynamic forces). Endothelial cells respond to these factors by expressing surface adhesion molecules, which, in turn, recruit circulating leukocytes and low-density lipoproteins containing cholesterol.[6] These events lead to the formation of atherosclerotic plaques, capable of narrowing parts of the coronary artery and impairing the blood flow to the myocardium. Depending on the speed of the plaque formation and the severity of the arterial obstruction, CAD can eventually culminate in myocardial infarction.[6]

Prompt and accurate diagnosis of CAD in at-risk subjects is vital to initiate an *ad hoc* therapy and avoid potential complications. Currently, coronary angiography stands as the most precise and widely accepted gold standard method for CAD diagnosis. However, this invasive procedure involves threading a catheter through an artery in the arm, neck, or upper thigh to reach the heart, accompanied by substantial costs and numerous potential side effects, including infections, catheterized artery damage, allergic reactions, and excessive bleeding. While computed tomographic coronary angiography offers a valid non-invasive alternative for exclusion of CAD in low- to intermediate-risk patients and for identification of severe stenosis in symptomatic patients, it is limited by a sensitivity of 50–70% with specificity of 83%.[7] An ideal test for CAD should be non-invasive, easy to perform, reproducible and sensitive. Blood tests fulfill these conditions and can readily be used to identify patients at risk for a specific disease. As such, considerable efforts have been invested in identifying biomarkers to aid in CAD risk prediction and diagnosis.[8,9] Despite the identification of several inflammatory biomarkers[10] with potential diagnostic utility,[11] none have yet been integrated into routine clinical practice. Therefore, there exists a pressing need for the development of novel, timely, and accurate CAD detection platforms. Herein, we tested our hypothesis that a nano-based blood test can act as an innovative and effective tool for CAD diagnosis.

In this approach, we take advantage of the formation of the protein corona (PC), a layer of biomolecules primarily composed of proteins that adsorb onto the surface of nanoparticles (NPs) when exposed to biological fluids. PCs have been widely investigated, often in a negative light, due to its role in altering the targeting efficacy and toxicity of therapeutic NPs.[12–17]

C. Corbo
University of Milano-Bicocca
Department of Medicine and Surgery
NANOMIB Center
Monza 20900, Italy
E-mail: claudia.corbo@unimib.it
C. Corbo
IRCCS Istituto Ortopedico Galeazzi
Milan 20161, Italy

Instead, in this study we harness the formation of PC around NPs for CAD diagnosis. A series of chemically diverse NPs is each used to capture different chemical subset of the plasma proteome, which has been shown to have specific alterations associated with various diseases.[18] When a particular NP is incubated with plasma from patients with various diseases, it yields disease-specific PCs.[19–21] The physical and chemical properties of NPs specifically render them ideal for biosensing[22] plasma proteins, including those present at low-concentration ones–a challenge for conventional detection methods. Such ability to detect low-abundance proteins has proven especially valuable in conditions like Alzheimer's Disease where relevant neurodegeneration-associated proteins circulate in extremely low concentrations. Indeed, PC-based analysis of plasma allowed discovery of protein markers associated with both asymptomatic stage of Alzheimer's Disease and its progression.[23] Such properties of PC have also been utilized recently to distinguish between sepsis and non-infectious systemic inflammation[24] and discover low-molecular weight and low-abundance cancer biomarkers.[25] 1D gel electrophoreses and densitometry analyses have also facilitated the detection of diseases such as pancreatic ductal adenocarcinoma[26] and glioblastoma multiforme.[27]

Profiling diseases by using multiple NPs has recently gained recognition as a means to gain deeper insight into diseased plasma[28] and achieve more precise proteomic profiling.[29] Building upon this multi-NP platform, several pilot studies have successfully differentiated plasma of breast and prostate cancer patients from that of healthy individuals.[30] In this context, we have recently expanded on this methodology to develop a PC-based sensor array nanosystem for early detection, discrimination, and prediction of Alzheimer's Disease.[31] We further refine these techniques to accurately detect the presence of atherosclerotic plaques by capturing the plasma proteomic changes resulting from its downstream biochemical signaling.[32,33] To the best of our knowledge, herein we present for the first time the application of the protein corona sensor array for the detection of CAD.[34]

2. Results and Discussion

The profile of adsorbed proteins in the PC is influenced by the type of material and the surface chemistry of NPs.[35] To detect a wider spectrum of plasma proteins, we designed a sensor array system employing six NPs with diverse chemical and physical features. We hypothesized that the incubation of the six distinct NPs in plasma would generate differential PC patterns that allow the computational discrimination between healthy individuals and those with CAD.

To this end, PCs were formed on various NP types with plasma obtained from three groups: i) CAD-diagnosed patients following coronary angiography (referred to as the CAD group), comprising $n_{cohort} = 15$ and $n_{noncohort} = 11$ individuals, ii) symptomatic patients without CAD following coronary angiography (the NO CAD group), consisting of $n_{noncohort} = 11$ individuals, and iii) healthy volunteers with no known cardiovascular disease risk factors (the CONTROL group), comprising $n_{cohort} = 15$, $n_{noncohort} = 10$ individuals. The cohort patients were included for longitudinal assessment.

A)

NPs	BARE			CAD			NO CAD			CONTROL		
	Size (nm)	SD	PDI	Size (nm)	SD	PDI	Size (nm)	SD	PDI	Size (nm)	SD	PDI
P	98.6	1.1	0.09	153.6	3.2	0.24	187.5	10.7	0.15	146.4	1.4	0.288
P-NH2	110.5	0.9	0.05	149.5	1.6	0.302	145.3	6.3	0.086	148.9	4	0.129
P-COOH	106.6	0.5	0.067	140.8	1.2	0.216	138.1	7.3	0.327	125.7	1.8	0.268
S	100.5	1.6	0.005	148.8	3.9	0.137	183.7	1.3	0.236	138.6	2.1	0.005
S-NH2	93.9	0.9	0.055	175.7	3.3	0.238	114.7	14.5	0.444	140.9	6.8	0.007
S-COOH	120	0.7	0.02	171.4	2.1	0.294	171.3	13.7	0.198	175.1	3.4	0.17

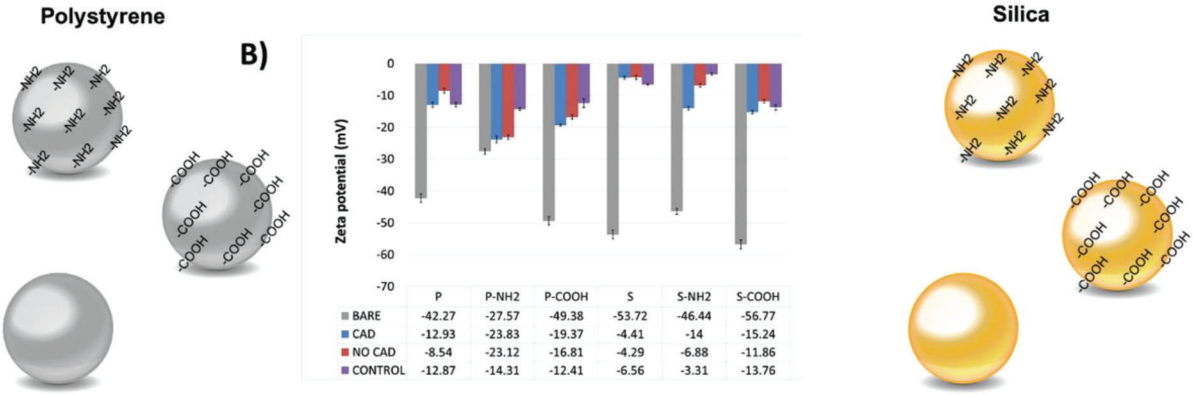

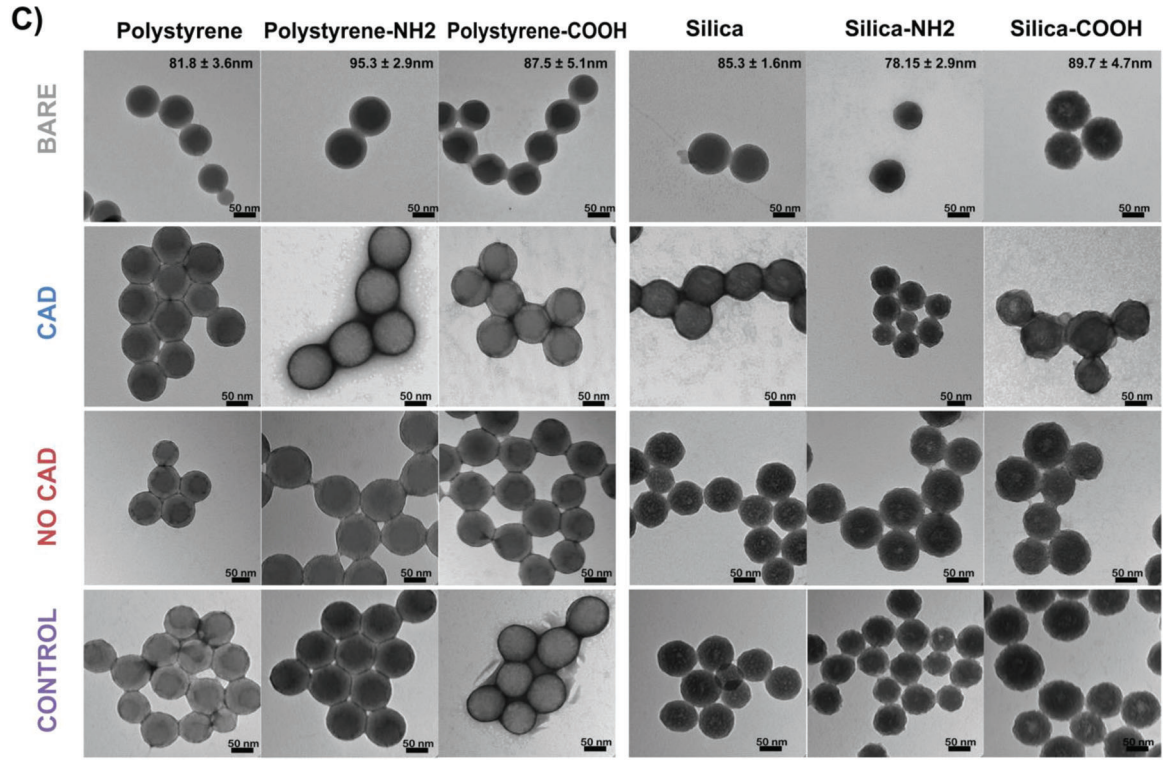

Figure 1. Physicochemical properties of the six NPs before and after incubation with three different plasmas (CAD, NO CAD, CONTROL). Silica (S) or polystyrene (P) NPs with either plain (P and S), amino-conjugated (P-NH2 and S-NH2), or carboxyl-conjugated (P-COOH and S-COOH) surfaces are reported. A) The size and polydispersity index (PDI) of the NPs in its bare form and PC-coated forms. PC-coated NPs exhibit an anticipated increase in both size (≈30-80 nm) and PDI (≈0.01-0.3), as expected. B) The surface charge (ζ-potential) before and after plasma incubation consistently increase for all NPs upon PC formation which is also expected. The increase in surface charge is most pronounced in S NPs and least pronounced in P-NH2 NPs. C) Morphological characterization of NPs before and after incubation with various CAD plasma samples, as analyzed by transmission electron microscopy (TEM). All NPs showed an increase in size upon PC formation and a thin layer of irregular edges can be observed in PC-coated NPs.

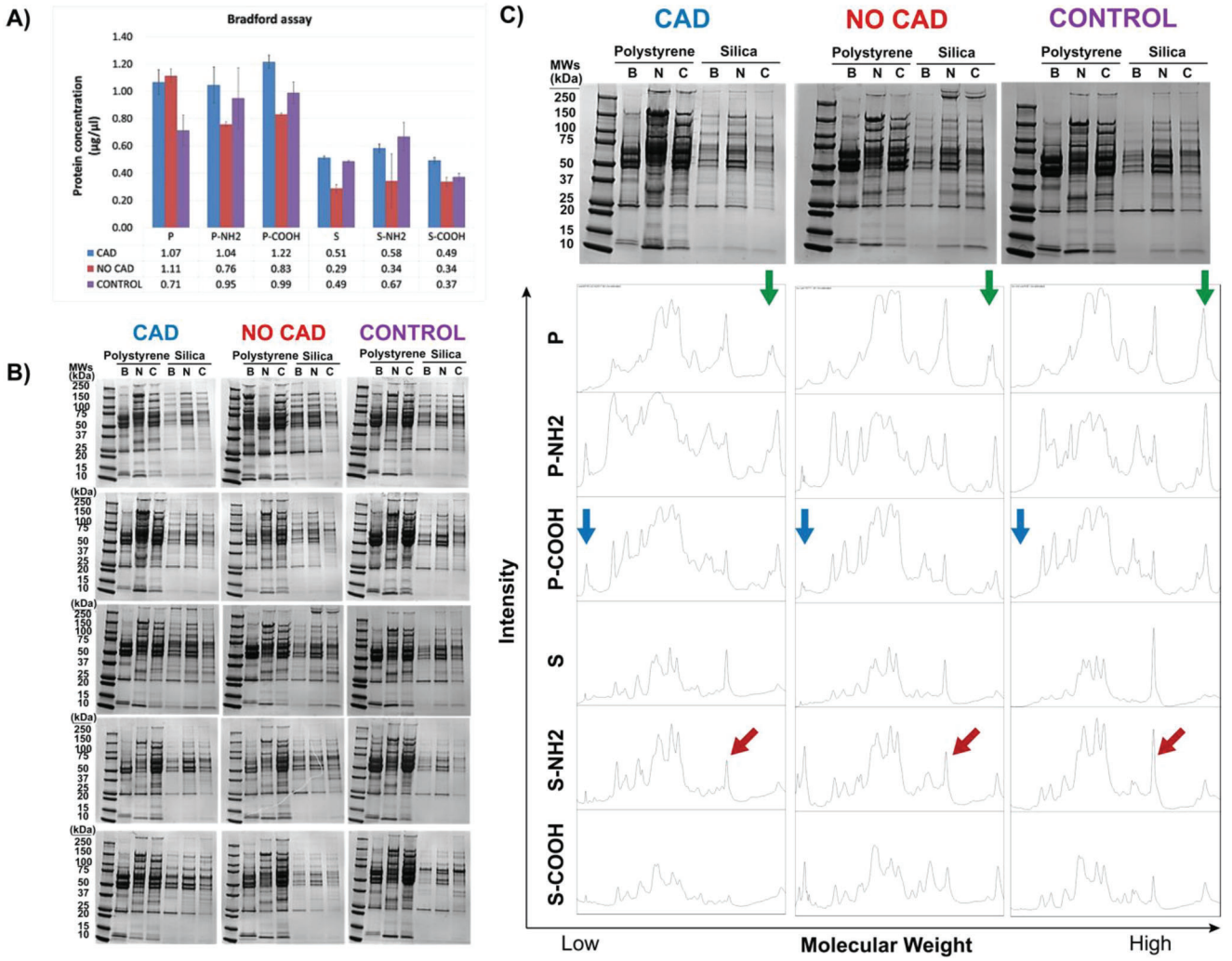

Figure 2. Protein characterization of PC profiles. A,B) PC profiles analyzed and compared via SDS-PAGE. Four representative gels of CAD, NO CAD, and CONTROL PCs are shown. Loading order: Polystyrene – B (Bare), Polystyrene – N (NH2), Polystyrene – C (COOH), Silica -B (Bare), Silica – N (NH2), Silica – C (COOH). C) Densitometric analysis was performed using ImageJ to quantify the band intensity for the SDS-PAGE gels for each PC. The y axis represents band intensity, while the x-axis displays molecular weight from high to low. Notable peaks have been highlighted as a visual confirmation of the variation in PC composition for each NP based on the type of plasma.

As mentioned above, we utilized six types of NPs: polystyrene (P) and silica (S), each with three surface modifications: none, amine (NH2) and carboxyl (COOH) (P, S, P-NH2, S-NH2, P-COOH, and S-COOH),[34] as depicted in **Figure 1**. The size, zeta potential, and morphology of NPs were measured before and after incubation in plasma to compare the synthetic identity of bare NPs to their corresponding biological counterparts (PC-coated NPs). Dynamic light scattering analysis revealed that bare NPs were all highly monodispersed, as demonstrated by polydispersity index ≤ 0.02 and a homogeneous size of ≈100 nm, ranging from 93 nm up to 120 nm (Figure 1A). After a 1-hour incubation with plasma of patients, all the NPs' sizes increased due to the adsorbed protein layer, the PC, whose thickness and composition depend on protein concentration, surface properties and NP size.[35] All bare NPs carried a negative surface charge (Figure 1B), with those amine-functionalized slightly less negative than others due to positive amine groups. These results aligned with supplier specifications and previous studies[36]: amine modification did not change net charge of both silica and polystyrene NPs, which remained negatively charged at physiological pH.

Upon exposure to plasma, owing to the charge characteristics of most plasma proteins at physiological pH,[37] the surface charges of all NPs became less negative with values ranging from −5 mV to −25 mV for chemically modified NPs and ≈−45 mV for bare NPs. Overall, all NPs increased in size and showed a less negative charge, regardless of the type of plasma and surface modification, upon formation of PC. Notably, however, P and S NPs exhibited a larger size increase (≈85 nm) when incubated with NO CAD plasma compared to when incubated with plasma from other conditions (40-50 nm). Conversely, the PC thickness of S-NH2 NPs incubated with CAD plasma was larger (≈40 nm) than those from other plasma types (≈15 nm). Transmission electron microscopy (TEM) confirmed that NPs retained their overall

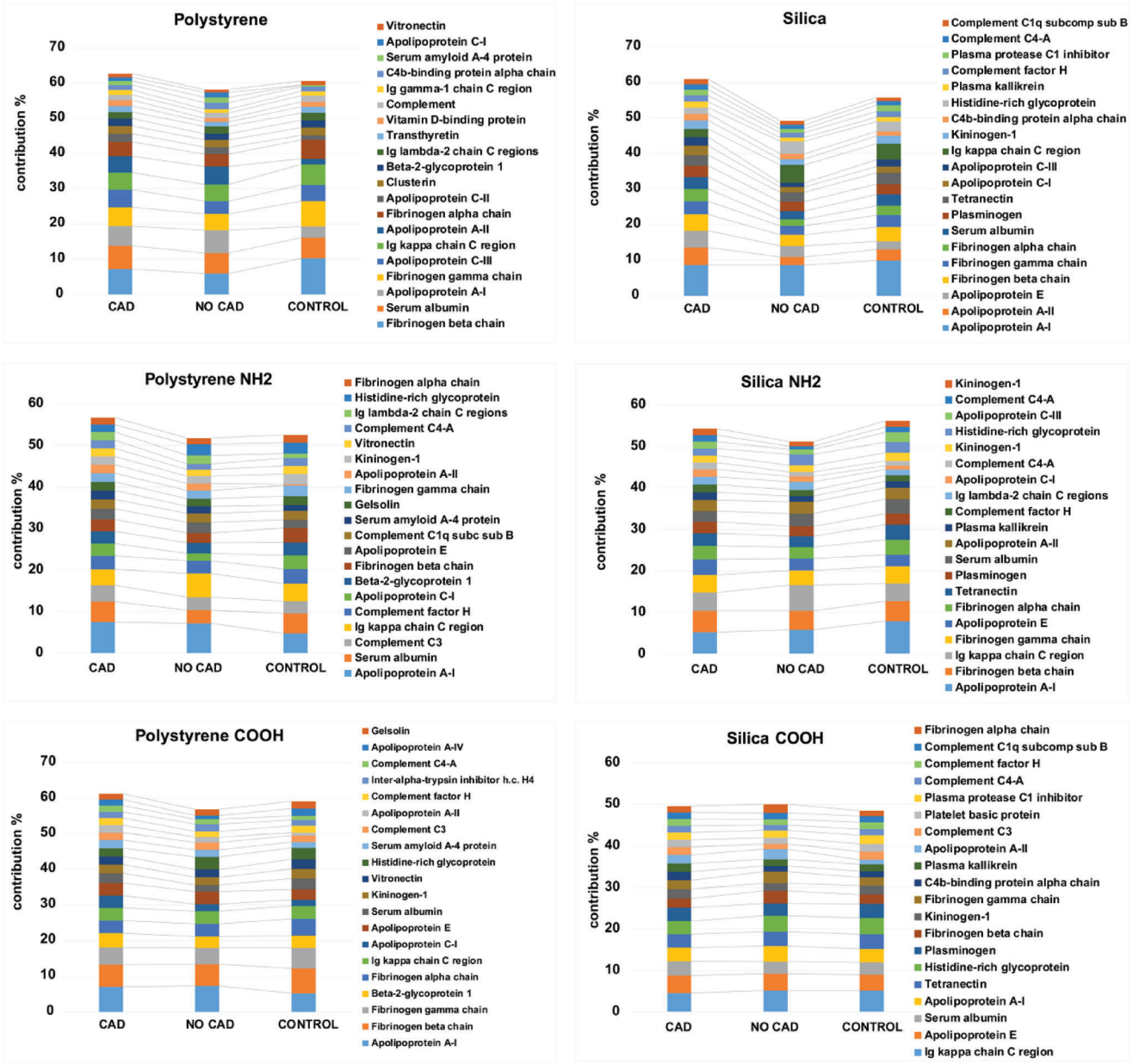

Figure 3. Differences in the percentage contribution of the top 20 most abundant proteins comprising the PCs for plasma, grouped by each NP. This is a visual representation of how different NP types attract different plasma proteins. The most abundant protein in the protein corona for polystyrene NPs is fibrinogen beta chain, while for silica-COOH NPs, it is the Ig kappa chain C region. For all other NPs, apolipoprotein A-1 is the most abundant. The figure also depicts how various plasma pathologies can influence the relative protein composition, even with the same NP, evident from the non-flat lines connecting the proteins for a given NP, underscoring the dynamic nature of the PC composition in different plasma conditions.

morphology and structure after plasma incubation (Figure 1C). Furthermore, an increase in the size after PC formation was observed directly via TEM, consistent with dynamic light scattering. We quantified protein concentrations in different PCs using Bradford assay, revealing that silica NPs adsorbed fewer proteins in the PC than polystyrene NPs (**Figure 2**A). This observation was consistent with Coomassie-stained 1D SDS-PAGE analyses of PCs (Figure 2B). Densitometry analysis of the SDS-PAGE gels revealed differences in protein amounts in the CAD, NO CAD, and CONTROL PCs of the same NP (Figure 2C, green and red arrows). In some cases, variations in the presence or absence of specific proteins were also observed (Figure 2C, blue arrows). Subsequently, we investigated the proteomic composition of the PCs by liquid chromatography with tandem mass spectrometry (LC-MS/MS) analysis, identifying more than 150 proteins in each PC-coated NP sample. From the LC-MS/MS analysis, spectral counts, which represent the total number of fragmentation spectra for all peptides attributed to a specific protein, were used to assess protein abundance and the percentage contribution of each identified proteins in the PCs (Figure S1, Supporting Information.

Table 1. Non-cohort sensitivity, specificity, and area under ROC curvet.

Array size	Sensitivity [%]	Specificity [%]	AUC [%]
One	80.0	77.8	86.23
	[53,94]	[38,95]	
Two	80.9	77.3	87.48
	[54,94]	[38,95]	
Three	81.3	79.5	88.71
	[55,94]	[40,95]	
Four	81.8	81.1	89.90
	[55,95]	[42,96]	
Five	82.1	82.0	90.58
	[56,95]	[43,96]	
Six	87.5	82.5	92.84
	[62,97]	[44,96]	

Classification accuracy for protein corona nanosystem with array size increasing from one to six nanoparticles (Column 1). Sensitivity and specificity, along with associated confidence intervals, improve with additional nanoparticles (Columns 2–3). Area under the receiver operating characteristic (ROC) curve also increases with array size (Column 4). Experimental results are averaged over 1000 independent draws of a training set comprising 16 plasmas, with evaluation on the remaining 16 plasmas. Mean values, along with 95% confidence intervals, are displayed.

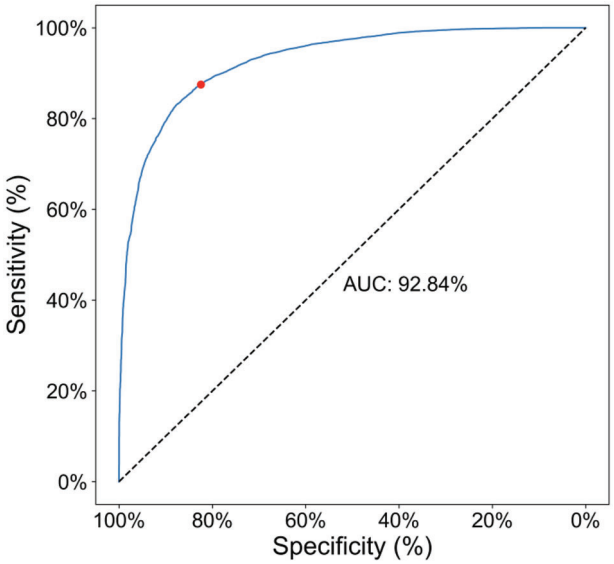

Figure 4. Performance of the full nanoparticle array on non-cohort distinguishing between CAD and NO CAD. Receiver operating characteristic (ROC) curve for full protein corona nanosystem with six nanoparticles on non-cohort samples is shown. Area under this curve is equal to 92.84%. The red point indicates the reported sensitivity and specificity, and the rest of the curve represents potential tradeoffs between sensitivity and specificity. Experimental results are averaged over 1000 independent draws of a training set comprising 16 plasmas, with evaluation on the remaining 16 plasmas.

Differences in the percentage contribution of the top 20 abundant proteins in the PCs are reported in **Figure 3**. The results highlighted correlations between PC composition, plasma condition, NP type, and surface modification.

We collected, analyzed, and classified data from all PC samples, creating a unique key for each measurement by combining NP, surface modification, plasma type, and label. Proteins identified with less than 2 peptides were excluded from analysis. TIBCO Spotfire Analyst 7.6.1 was used to pivot the data such that rows represented protein accession, columns were sorted by the key, and individual cell values contained the percentage contribution (Figure S2, Supporting Information).

We investigated whether the PC fingerprint of various NPs could be used to recognize signature proteomic patterns associated with different physiologic conditions (i.e., biosensors). To robustly test this hypothesis, we classified the entire protein dataset using a random forest classification base package from SKlearn. We tested the accuracy of our classifier in discriminating between patients by analyzing 16 blind plasma samples. For each plasma sample PCs were formed around the six NPs in our PC sensor array nanosystem. Proteins within the PCs were identified by LC-MS/MS, and the results were analyzed using the previously mentioned classification and clustering methods.

We first measured the sensitivity (87.5%) and specificity (82.5%) for the random forest classifier's ability to distinguish between blind non-cohort (no longitudinal aspect) samples of CAD and NO CAD (**Table 1**). Results were averaged over 1000 independent training sets consisting of 16 plasma samples, with evaluations on the remaining 16 samples, and are reported with 95% confidence intervals. The corresponding receiver operating characteristic (ROC) curve is shown in **Figure 4**, illustrating the achievable range of sensitivity and specificity with the red indicating the point of maximum benefit. The area under the curve (AUC) of the ROC plot served as a proxy for accuracy in the classification task (92.84%). We also demonstrated that with more sensor array elements (NPs), sensitivity, specificity, and AUC all increased (Table 1). To further characterize the model with varying sensor array elements, the p-values for sensitivity and specificity in comparison to the null hypotheses were generated using a one-sided Wilcoxon signed-ranked test (**Table 2**). We find that the p-values for the sensitivity and specificity increased or remained the same with a sensor array $n < 6$.

We then measured the sensitivity (80.3%), specificity (70.4%), and AUC (84.17%) for the classifier's ability to distinguish between blind cohort samples of CAD and CONTROL (**Figure 5**). We also demonstrated that the model's sensitivity and specificity

Table 2. *Non-cohort* statistical comparison of sensitivity and specificity between arrays with different numbers of nanoparticles. *P*-values for the null hypotheses that arrays with fewer than six nanoparticles achieve the same, or greater, sensitivity (Column 1) and specificity (Column 2) as the array with all six nanoparticles. Testing was performed using a one-sided Wilcoxon signed-rank test. Each null hypothesis individually can be rejected at a 99% significance level, and moreover the entire set of 10 null hypotheses can be rejected via a Benjamini-Hochberg procedure, with false discovery rate controlled at 1%.

Array size	Sensitivity	Specificity
One	6.8×10^{-93}	1.2×10^{-23}
Two	2.0×10^{-96}	2.0×10^{-32}
Three	5.0×10^{-100}	1.3×10^{-15}
Four	5.2×10^{-88}	4.7×10^{-06}
Five	3.8×10^{-69}	3.0×10^{-03}

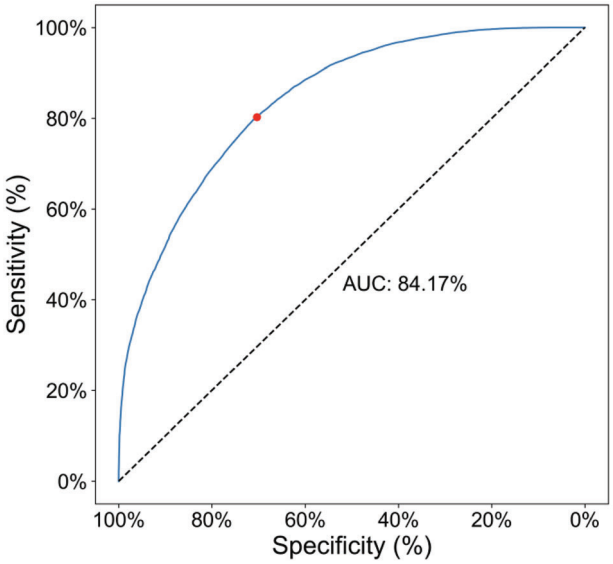

Figure 5. Performance of the full nanoparticle array on cohort distinguishing between CAD and CONTROL. The receiver operating characteristic (ROC) curve for full protein corona nanosystem with six nanoparticles on cohort samples is shown. Area under this curve is equal to 84.17%. The red point indicates the reported sensitivity and specificity, and the rest of the curve represents potential tradeoffs between sensitivity and specificity. Experimental results are averaged over 1000 independent draws of a training set comprising 16 non-cohort (CAD and NO CAD) plasmas, with evaluation on all 30 cohort (CAD and CONTROL) plasmas.

for distinguishing CAD from CONTROL increased proportionally with the number of elements in the sensor array (**Table 3**), mirroring the analysis conducted for CAD versus NO CAD as described earlier. The results were averaged over 1000 independent draws with a training set of 16 non-cohort plasmas with evaluation on all 30 cohort plasmas. Remarkably, the cohort analysis achieved a substantial accuracy even when trained on non-cohort plasma samples.

The random forest classifier model generated an importance score for each protein-NP pair, indicating the contribution of the pair to the decision tree branch. The importance score for the top 30 highest scoring proteins was plotted, revealing distinct contribution from each NP for each protein (**Figure 6**), demonstrating the robustness of the model in distinguishing proteins based on the unique physicochemical properties of the NPs variably contributing to the classification task. The top 30 highest scoring proteins that were detected on all six NPs in the non-cohort plasmas and are listed in Figure 6. These proteins that contributed most to the classification task interestingly include Apolipoprotein (a) and the complement components which are directly and indirectly related to CAD pathogenesis. For instance, complement activation has been associated with atherosclerosis development, plaque rupture, and thrombosis.[38] Apolipoprotein (a), known to be an attractive biomarker candidate for use into clinical practice for CAD, is the main component of lipoprotein (a), it undergoes proteolytic cleavage, and its fragments accumulate in atherosclerotic plaques.[39] These results confirm the capability of our sensor array technology to perform the classification task on pathologically and biologically relevant grounds. Interestingly, beyond several known CAD-related biomarkers, our top 30 list includes potential novel biomarkers warranting further investigation.

3. Conclusion

In this work, by combining a sensor array-based diagnostic approach with personalized PCs, we designed a novel diagnostic CAD test to be used as a non-invasive alternative screening option for high-risk patients. Sensor array technologies involve a range of sensor elements used to create a unique identifier for each analyte, facilitating precise analyte recognition through pattern recognition. The use of sensor arrays has been reported for the detection of different analytes such as foods, beverages, gases, biomolecules, and NPs.[40–45] NP-based sensor arrays provide an attractive alternative approach to current research efforts in searching for specific biomarkers for disease detection.[46] Herein, we harnessed this approach, incorporating six NPs as sensor elements to exploit disease-specific PCs for CAD diagnostics.

Our results indeed demonstrate that this approach can discriminate between plasma of CAD patients and healthy individuals, as well as distinguish between cohort and non-cohort patients. This positions this sensor array platform as a promising diagnostic tool for non-invasive, blood-based CAD detection with accuracy and precision.

In conclusion, in this work we showcase the capability of a six-NP PC sensor array in CAD detection with a sensitivity of 87.5%, specificity of 82.5%, and accuracy of 92.84%, which outperforms CT coronary angiography, the current best alternative to invasive coronary angiogram. Moreover, the PC sensor array nanosystem demonstrates the ability to discriminate both CAD patients from symptomatic patients at risk for CAD, as well as CAD patients

Table 3. Cohort sensitivity, specificity, and area under ROC curve. Classification accuracy for protein corona nanosystem with array size increasing from one to six nanoparticles (Column 1). Sensitivity and specificity, along with associated confidence intervals, improve with additional nanoparticles (Columns 2–3). Area under the receiver operating characteristic (ROC) curve also increases with array size (Column 4). Experimental results are averaged over 1000 independent draws of a training set comprising 16 non-cohort plasmas, with evaluation on all 30 cohort plasmas. Mean values, along with 95% confidence intervals, are displayed.

Array size	Sensitivity [%]	Specificity [%]	AUC [%]
One	47.3	71.1	63.79
	[31,64]	[51,84]	
Two	64.9	67.4	72.98
	[46,79]	[48,81]	
Three	70.6	69.5	77.23
	[51,84]	[50,83]	
Four	74.7	70.5	80.17
	[55,87]	[50,84]	
Five	78.1	69.9	82.20
	[58,90]	[49,85]	
Six	80.3	70.4	84.17
	[59,92]	[49,86]	

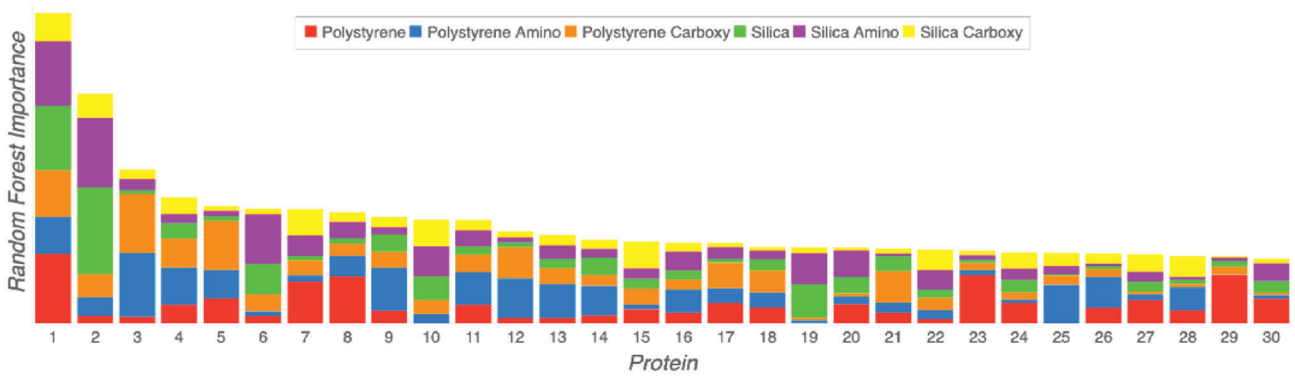

Importance	Accession	Description	Importance	Accession	Description
1	P02647	Apolipoprotein A-I	16	P07360	Complement component C8 gamma chain
2	P06727	Apolipoprotein A-IV	17	P49908	Selenoprotein P
3	P01024	Complement C3	18	P02748	Complement component C9
4	P07357	Complement component C8 alpha chain	19	P36955	Pigment epithelium-derived factor
5	P00747	Plasminogen	20	P06396	Gelsolin
6	P0C0L4	Complement C4-A	21	P01861	Ig gamma-4 chain C region
	P0C0L5	Complement C4-B		P01859	Ig gamma-2 chain C region
7	P02654	Apolipoprotein C-I	22	P60709	Actin, cytoplasmic 1
8	P02652	Apolipoprotein A-II		P63261	Actin, cytoplasmic 2
9	P09871	Complement C1s subcomponent	23	P02655	Apolipoprotein C-II
10	P00746	Complement factor D	24	P04004	Vitronectin
11	P01023	Alpha-2-macroglobulin	25	P05019	Insulin-like growth factor I
12	P10909	Clusterin	26	P04114	Apolipoprotein B-100
13	P13671	Complement component C6	27	P02649	Apolipoprotein E
14	P00736	Complement C1r subcomponent	28	P00748	Coagulation factor XII
15	P01766	Ig heavy chain V-III region BRO	29	P02765	Alpha-2-HS-glycoprotein
	P01777	Ig heavy chain V-III region TEI	30	P08603	Complement factor H

Figure 6. Protein importance for classification (non-cohort). Each column indicates the classification importance of a specific protein. The six colored stacks within a column for a given protein correspond to the importance of the observed interaction of that protein with each of the three nanoparticles. Information on the most important overall proteins, detected on combinations of all six nanoparticles in the non-cohort plasmas is reported in the table.

from healthy CONTROL cohort patients, further highlighting its potential in clinical settings. The ease of a blood-based test with no side effect has immense potential to reduce CAD complication via early detection and more frequent testing. Interestingly, our group has already successfully tested the approach presented here on Alzheimer's disease (30) and, due to its versatility, we envision that may be utilized also for the detection of other various human diseases in need of more biomarkers, early detection methods, or less invasive diagnostic procedures. Potential applications include, but are not limited to, musculoskeletal disorders (e.g., prediction of bone metastasis, therapeutic evaluation of osteosarcoma).

4. Experimental Section

Nanoparticles: Three differently functionalized silica particles were purchased by Kisker-Products (https://www.kisker-biotech.com/); three differently functionalized polystyrene particles were purchased by Polyscience, Inc. (http://www.polysciences.com/). All the particles had the same size (100 nm). Their morphology, average size, polydispersity index (PDI), and zeta potential were characterized by TEM, DLS and zeta potential measurements.

Protein Corona Formation: Human plasma was collected from healthy subjects, CAD+ and CAD- patients at the Dept Cardiology, Athens, Euroclinic, Athens, Greece. IRB approval and informed consent were provided. The PCs were created by incubating 0.5 mg of NPs in 200 µL deionized H_2O diluted with the 200 µL of thawed aliquoted human plasma. Incubation was performed in 37 °C under agitation for 1 h. Immediately after incubation, centrifugation was executed at 14000 rpm and 10 °C for 30 min to form a pellet. Next, the pellet was washed and suspended in 200 µl of phosphate-buffered saline (PBS) at 4 °C. The centrifugation was repeated three times, again at 14000 rpm and 10 °C for 30 min. The pellet of the PC-coated NPs was either resuspended in a solution of 8 M Urea 50 mM ammonium bicarbonate for SDS-PAGE gels and liquid chromatography with tandem mass spectrometry analysis, or in deionized H_2O for size and ζ-potential nanoparticle characterization.

Nanoparticles Characterization: Size and ζ-potential of bare and protein corona-coated nanoparticles have been characterized by diluting 10 µl of each sample in 1 ml total of distilled water. Measurements have been performed using a Zetasizer Nano ZS90 (Malvern, UK). Size and surface charge values were given as mean ± S.D. of three independent measurements.

Protein Concentration Assay: The amount of proteins within the corona was determined by Bradford assay (Bio-rad) using bovine serum albumin at a known concentration as the standard to build a 5-point standard curve ($R^2 = 0.99$). Protein concentrations were recorded as an average of three experiments ± S.D.

1D-SDS PAGE Gels: Proteins in the corona were dissolved in in 8 M Urea, 50 mM ammonium bicarbonate. An equal amount of Laemmli buffer 2X was added to the pellet and heated for 5 min at 90 °C before being loaded and resolved onto a 4–20% Mini-PROTEAN® TGX™ Precast Gels (Bio-Rad Laboratories, Hercules, CA) for 1 h at 120 V. Proteins were stained with Coomassie Brilliant Blue (Fisher Scientific, Fair Lawn, NJ, USA) overnight followed by extensive washing in ultra-pure water.

Mass Spectrometry–Reduction, Alkylation, and Tryptic Digestion: Proteins were reduced with 10 mM dithiothreitol (Sigma) for 1 h at 56 °C and then alkylated with 55 mM iodoacetamide (Sigma) for 1 h at 25 °C in the dark. Proteins were then digested with modified trypsin (Promega) at an enzyme/substrate ratio of 1:50 in 100 mM ammonium acetate, pH 8.9 at 25 °C overnight. Trypsin activity was halted by addition of acetic acid (99.9%, Sigma) to a final concentration of 5%. Peptides were desalted using C18 SpinTips (Protea, Morgantown, WV) then vacuum centrifuged and stored at −80 °C.

Mass Spectrometry–LC-MS/MS: Peptides were separated by reverse phase HPLC (Thermo Easy nLC1000) using a pre-column (made in-house, 6 cm of 10 µm C18) and a self-pack 5 µm tip analytical column (12 cm of 5 µm C18, New Objective) over a 140-minute gradient before nanoelectrospray using a QExactive mass spectrometer (Thermo). Solvent A was 0.1% formic acid and solvent B was 80% MeCN/0.1% formic acid. The gradient conditions were 2–10% B (0-3 min), 10–30% B (3-107 min), 30–40% B (107-121 min), 40–60% B (121-126 min), 60–100% B (126-127 min), 100% B (127-137 min), 100-0% B (137-138 min), 0% B (138-140 min), and the mass spectrometer was operated in a data-dependent mode. The parameters for the full scan MS were: resolution of 70000 across 350–2000 m/z, AGC 3e6, and maximum IT 50 ms. The full MS scan was followed by MS/MS for the top 10 precursor ions in each cycle with a normalized collision energy of 28 and dynamic exclusion of 30 s. Raw mass spectral data files (.raw) were searched using Proteome Discoverer (Thermo) and Mascot version 2.4.1 (Matrix Science). Mascot search parameters were: 10 ppm mass tolerance for precursor ions; 15 mmu for fragment ion mass tolerance; 2 missed cleavages of trypsin; fixed modification was carbamidomethylation of cysteine; variable modification was methionine oxidation. Only peptides with a Mascot score greater than or equal to 25 were included in the data analysis. Spectral counting was performed by summing the total number of peptides selected for fragmentation of each protein.

Statistics: All statistical analyses were performed in Python, and figures and graphs were created using the bokeh package in Python, along with Microsoft Excel, XLSTAT, and MATLAB. For all plasma samples, a data matrix X_i was generated such that each row of the matrix corresponded to the protein abundances of a single nanoparticle, as obtained from the protein corona nanoplatform. As a preprocessing step, the protein abundances were converted to relative protein abundances by normalizing the rows of all of the matrices.

Supporting Information

Supporting Information is available from the Wiley Online Library or from the author.

Acknowledgements

The research conducted in this manuscript was supported by the Italian Ministry of Health, Ricerca Corrente 2022, project RC L2089 by the University of Milano Bicocca, project 2019-ATE-0254, and project 2018-ATE-0400 to C.C.

Conflict of Interest

The authors declare no conflict of interest.

Author Contributions

G.Y.L. and C.C. conducted the experiments; I.M., A.L., and D.F. provided machine learning and statistical analysis; D.K., and Y.P. provided clinical insights and guidance on the cohort data; T.P. and P.M. provided technical support; R.M., F.S., W.T., and F.T. provided conceptual advice and revised the paper; G.Y.L. and C.C. wrote the paper and revised it according to the comments of authors; C.C. designed the experiments, directed the project, and provided mentoring.

Data Availability Statement

The data that support the findings of this study are available from the corresponding author upon reasonable request.

Keywords

cardiovascular disease detection, nano-assay, nanomedicine, protein corona, sensor arrays

Received: July 21, 2023
Revised: September 26, 2023
Published online:

[1] S. Yusuf, S. Reddy, S. O. Unpuu, S. Anand, *Circulation* **2001**, *104*, 2746.
[2] G. A. Roth, G. A. Mensah, C. O. Johnson, G. Addolorato, E. Ammirati, L. M. Baddour, N. C. Barengo, A. Z. Beaton, E. J. Benjamin, C. P. Benziger, A. Bonny, M. Brauer, M. Brodmann, T. J. Cahill, J. Carapetis, A. L. Catapano, S. S. Chugh, L. T. Cooper, J. Coresh, M. Criqui, N. Decleene, K. A. Eagle, S. Emmons-Bell, V. L. Feigin, J. Fernández-Solà, G. Fowkes, E. Gakidou, S. M. Grundy, F. J. He, G. Howard, et al., *J. Am Coll. Cardiol.* **2020**, *76*, 2982.
[3] M. A. Khan, M. J. Hashim, H. Mustafa, M. Y. Baniyas, S. K. B. M. Al Suwaidi, R. Alkatheeri, F. M. K. Alblooshi, M. E. A. H. Almatrooshi, M. E. H. Alzaabi, R. S. Al Darmaki, S. N. A. H. Lootah, *Cureus* **2020**, *12*, e9349.
[4] E. J. Benjamin, M. J. Blaha, S. E. Chiuve, M. Cushman, S. R. Das, R. Deo, S. D. De Ferranti, J. Floyd, M. Fornage, C. Gillespie, C. R. Isasi, M. C. Jiménez, L. C. Jordan, S. E. Judd, D. Lackland, J. H. Lichtman, L. Lisabeth, S. Liu, C. T. Longenecker, R. H. Mackey, K. Matsushita, D. Mozaffarian, M. E. Mussolino, K. Nasir, R. W. Neumar, L. Palaniappan, D. K. Pandey, R. R. Thiagarajan, M. J. Reeves, M. Ritchey, et al., *Circulation* **2017**, *135*, e146.
[5] D. C. E. Bloom, E. Jané-Llopis, S. Abrahams-Gessel, L. Bloom, S. Fathima, A. Feigl, *Program on the Global Demography of Aging* **2012**.
[6] D. Tousoulis, M. Charakida, C. Stefanadis, *Heart* **2006**, *92*, 368.
[7] M. Doris, D. E. Newby, *Curr. Cardiol. Rep.* **2016**, *18*, 18.
[8] A. S. Jaffe, L. Babuin, F. S. Apple, *J. Am Coll. Cardiol.* **2006**, *48*, 1.
[9] L. Anderson, *J. Physiol.* **2005**, *563*, 23.
[10] G. K. Hansson, A. Hermansson, *Nat. Immunol.* **2011**, *12*, 204.
[11] E. Zakynthinos, N. Pappa, *J. Cardiol.* **2009**, *53*, 317.
[12] G. Caracciolo, O. C. Farokhzad, M. Mahmoudi, *Trends Biotechnol.* **2017**, *35*, 257.
[13] C. Corbo, R. Molinaro, A. Parodi, N. E. Toledano Furman, F. Salvatore, E. Tasciotti, *Nanomedicine (Lond)* **2016**, *11*, 81.

[14] E. Tasciotti, R. Molinaro, F. Taraballi, N. Toledano Furman, M. Sherman, A. Parodi, F. Salvatore, C. Corbo, *Int J Nanomedicine* **2016**, *11*, 3049.
[15] C. Corbo, R. Molinaro, F. Taraballi, N. E. Toledano Furman, K. A. Hartman, M. B. Sherman, E. De Rosa, D. K. Kirui, F. Salvatore, E. Tasciotti, *ACS Nano* **2017**, *11*, 3262.
[16] M. Mahmoudi, S. N. Saeedi-Eslami, M. A. Shokrgozar, K. Azadmanesh, M. Hassanlou, H. R. Kalhor, C. Burtea, B. Rothen-Rutishauser, S. Laurent, S. Sheibani, H. Vali, *Nanoscale* **2012**, *4*, 5461.
[17] M. Mahmoudi, I. Lynch, M. R. Ejtehadi, M. P. Monopoli, F. B. Bombelli, S. Laurent, *Chem. Rev.* **2011**, *111*, 5610.
[18] S. M. Hanash, S. J. Pitteri, V. M. Faca, *Nature* **2008**, *452*, 571.
[19] C. Corbo, R. Molinaro, M. Tabatabaei, O. C. Farokhzad, M. Mahmoudi, *Biomater. Sci.* **2017**, *5*, 378.
[20] M. J. Hajipour, S. Laurent, A. Aghaie, F. Rezaee, M. Mahmoudi, *Biomater. Sci.* **2014**, *2*, 1210.
[21] M. J. Hajipour, J. Raheb, O. Akhavan, S. Arjmand, O. Mashinchian, M. Rahman, M. Abdolahad, V. Serpooshan, S. Laurent, M. Mahmoudi, *Nanoscale* **2015**, *7*, 8978.
[22] A. P. F. Turner, B. Chen, S. A. Piletsky, *Clin. Chem.* **1999**, *45*, 1596.
[23] M. Hadjidemetriou, J. Rivers-Auty, L. Papafilippou, J. Eales, K. A. B. Kellett, N. M. Hooper, C. B. Lawrence, K. Kostarelos, *ACS Nano* **2021**, *15*, 7357.
[24] L. Papafilippou, A. Claxton, P. Dark, K. Kostarelos, M. Hadjidemetriou, *Nanoscale* **2020**, *12*, 10240.
[25] M. Hadjidemetriou, Z. Al-Ahmady, M. Buggio, J. Swift, K. Kostarelos, *Biomaterials* **2019**, *188*, 118.
[26] L. Digiacomo, D. Caputo, R. Coppola, C. Cascone, F. Giulimondi, S. Palchetti, D. Pozzi, G. Caracciolo, *Biointerphases* **2021**, *16*, 011010.
[27] R. Di Santo, E. Quagliarini, L. Digiacomo, D. Pozzi, A. Di Carlo, D. Caputo, A. Cerrato, C. M. Montone, M. Mahmoudi, G. Caracciolo, *Biomater. Sci.* **2021**, *9*, 4671.
[28] M. Del Pilar Chantada-Vázquez, A. C. López, M. G. Vence, S. Vázquez-Estévez, B. Acea-Nebril, D. G. Calatayud, T. Jardiel, S. B. Bravo, C. Nuez, *J. Proteomics* **2020**, *212*, 103581.
[29] J. E. Blume, W. C. Manning, G. Troiano, D. Hornburg, M. Figa, L. Hesterberg, T. L. Platt, X. Zhao, R. A. Cuaresma, P. A. Everley, M. Ko, H. Liou, M. Mahoney, S. Ferdosi, E. M. Elgierari, C. Stolarczyk, B. Tangeysh, H. Xia, R. Benz, A. Siddiqui, S. A. Carr, P. Ma, R. Langer, V. Farias, O. C. Farokhzad, *Nat. Commun.* **2020**, *11*, 3662.
[30] L. Digiacomo, K. Jafari-Khouzani, S. Palchetti, D. Pozzi, A. L. Capriotti, A. Laganà, R. Zenezini Chiozzi, D. Caputo, C. Cascone, R. Coppola, G. Flammia, V. Altomare, A. Grasso, M. Mahmoudi, G. Caracciolo, *Nanoscale* **2020**, *12*, 16697.
[31] C. Corbo, A. A. Li, H. Poustchi, G. Y. Lee, S. Stacks, R. Molinaro, P. Ma, T. Platt, S. Behzadi, R. Langer, V. Farias, O. C. Farokhzad, *Adv. Healthcare Mater.* **2021**, *10*, e2000948.
[32] P. Májek, Z. Reicheltová, J. Suttnar, M. Malý, M. Oravec, K. PecNková, J. E. Dyr, *J. Transl. Med.* **2011**, *9*, 84.
[33] P. M. Ridker, C. H. Hennekens, J. E. Buring, N. Rifai, *N. Engl. J. Med.* **2000**, *342*, 836.
[34] O. C. Farokhzad, M. Mahmoudi, C. Corbo, System and method for protein corona sensor array for early detection of diseases, **2023**.
[35] M. Lundqvist, J. Stigler, G. Elia, I. Lynch, T. Cedervall, K. A. Dawson, *Proc. Natl. Acad. Sci. U. S. A.* **2008**, *105*, 14265.
[36] S. Tenzer, D. Docter, J. Kuharev, A. Musyanovych, V. Fetz, R. Hecht, F. Schlenk, D. Fischer, K. Kiouptsi, C. Reinhardt, K. Landfester, H. Schild, M. Maskos, S. K. Knauer, R. H. Stauber, *Nat. Nanotechnol.* **2013**, *8*, 772.
[37] C. D. Walkey, W. C. W. Chan, *Chem. Soc. Rev.* **2012**, *41*, 2780.
[38] A. M. Carter, *Scientifica (Cairo)* **2012**, 402783.
[39] J. E. Fortunato, H. S. Bassiouny, R. H. Song, H. Kocharian, S. Glagov, C. Edelstein, A. M. Scanu, *J. Vasc. Surg.* **2000**, *32*, 555.
[40] N. A. Rakow, K. S. Suslick, *Nature* **2000**, *406*, 710.
[41] R. F. Machado, D. Laskowski, O. Deffenderfer, T. Burch, S. Zheng, P. J. Mazzone, T. Mekhail, C. Jennings, J. K. Stoller, J. Pyle, J. Duncan, R. A. Dweik, S. C. Erzurum, *Am J. Respir. Crit. Care Med.* **2005**, *171*, 1286.
[42] D. S. Lee, J. K. Jung, J. W. Lim, J. S. Huh, D. D. Lee, *Sens. Actuators, B* **2001**, *77*, 228.
[43] M. Mahmoudi, S. E. Lohse, C. J. Murphy, K. S. Suslick, *ACS Sens.* **2016**, *1*, 17.
[44] J. R. Askim, M. Mahmoudi, K. S. Suslick, *Chem. Soc. Rev.* **2013**, *42*, 8649.
[45] A. Star, V. Joshi, S. Skarupo, D. Thomas, J.-C. P. Gabriel, *J. Phys. Chem. B* **2006**, *110*, 21014.
[46] N. D. Le, M. Yazdani, V. M. Rotello, *Nanomedicine (Lond)* **2014**, *9*, 1487.